On the Antenna Position to Improve the Radiation Pattern Characterization

Nicolas Mezieres, Benjamin Fuchs, Laurent Le Coq, Jean-Marie Lerat, Romain Contreres, Gwenn Le Fur

On the Antenna Position to Improve the Radiation Pattern Characterization

Nicolas Mézières, Benjamin Fuchs, *Senior Member, IEEE*, Laurent Le Coq, Jean-Marie Lerat, Romain Contreres and Gwenn Le Fur

***Abstract*—The 3D characterization of radiating structures is a frequently encountered, and yet challenging, procedure. The theoretical sampling criterion often leads to prohibitive measurement duration, especially for antennas embedded on electrically large structures. However, the position of the antenna under test strongly influences the sampling requirements. By appropriately positioning the antenna with respect to the measurement system, it is possible to promote the low spatial frequency part of its spherical harmonic spectrum. We present a post-processing optimization algorithm enabling a systematic and accurate determination of the antenna *best* position from a given measurement dataset with no prior knowledge. This so-optimized position is exploited to improve the characterization of the antenna radiation pattern without resorting to any additional measurement sample. The proposed algorithm is validated for both near-field simulations and far-field measurements on various radiating structures, including an antenna embedded on a satellite model.**

***Index Terms*—Antenna measurements, antenna radiation patterns, optimization methods, spherical vector wave expansion, sparse recovery**

I. Introduction

THE use of Vector Spherical Harmonic (VSH) expansion is widely spread in the antenna measurement community as a powerful tool for antenna characterization. The VSH spectrum indeed encompasses many valuable physical informations about the radiated field that deserve to be fully exploited. The underlying theory behind VSH and its application to antenna measurements are now well established [1]. Moreover, spherical near-field measurements of antennas are known to be a very accurate characterization technique [2], [3]. The analytical nature of the VSH allows for exact operations on moving or rotating electromagnetic sources from a given, eventually discrete, electric field [1]. More explicitly, the VSH spectrum provides an identity card of the antenna's radiated field relatively to a given coordinate system. It means that both position and orientation of the antenna in the coordinate system change its VSH expansion. In other words, a given radiating structure will have different spectra depending on the origin from which the VSH are computed.

Manuscript received 12, 2020; revised 01, 2021.

This work was carried out in the frame of a CNES and LNE grant and is supported in part by the European Union through the European Regional Development Fund (ERDF), and by the french region of Brittany, Ministry of Higher Education and Research, Rennes Métropole and Conseil Départemental 35, through the CPER Project SOPHIE / STIC & Ondes.

N. Mézières is with the IETR, CNES and LNE (e-mail: nicolas.mezieres@univ-rennes1.fr). B. Fuchs and L. Le Coq are with the IETR, UMR CNRS 6164, Rennes, France. J.-M. Lerat is with the LNE, Trappes, France. R. Contreres and G. Le Fur are with the CNES, Toulouse, France.

Digital Object Identifier

The impact of the antenna position on its associated spectrum is known [4] and several studies have been led to provide relevant locations or to adapt the near-field technique consequently, allowing to reduce the impact of the tested device positioning [5]–[8]. The key point is to concentrate the spectrum to low spatial or angular frequency content, or slowly varying VSH, as it is then easier to properly expand the antenna pattern. The *best* position can thus be defined as the coordinate system origin achieving the highest concentration in the low-degree part of the VSH spectrum, for which an appropriate metric is adapted thereafter. More particularly, two iterative approaches have been proposed on position optimization in post-processing. The first one, [9], deals with fast measurements procedures, and emphasizes on minimizing the number of significant modes to improve the field reconstruction accuracy according to the sparse recovery theory [10]. Indeed, the reconstruction accuracy from a low density sample is linked to the number of significant modes in the expansion, as shown in [11]–[14]. However, the distribution of the significant modes over the spectrum also has an important role in this matter. The second method in [15] works over this power distribution over the spectrum to estimate a radiation center, that corresponds to the phase center in the case of antennas having a single main beam. A fixed perturbation in the 6 directions of the current position (the 3 Cartesian ones in two ways each) is applied with a fixed step. The origin is then moved in the direction leading to the best power concentration within a predetermined low frequency part of the spectrum.

The radiating structure under test cannot always be positioned at will in the measurement system because of cinematic or weight reasons, constituting the main motivation point of previous works [7], [8]. Besides, the field sampling strategy has to comply to the practical constraints imposed by the measurement system. Finally, the perfect knowledge of the antenna position in the measurement system does not necessarily tell us where to place it at best because of possible interactions. All these reasons impact the antenna measurement procedure and have led us to propose the following antenna measurement post-processing approach.

Our main idea is to exploit as much as possible the information contained in the measured data using VSH expansion. We propose a procedure to automatically determine the *best* antenna position by appropriately post-processing the measured near or far field and without resorting to any additional information as compared to a standard measurement procedure. This position is used to post-process the available measurement samples without performing any

additional measurements to reconstruct the radiated field in the initial coordinate system, as explained in [8], [9]. The iterative algorithm enables a minimization of the number of significant coefficients required to describe the field and more particularly to concentrate the power distribution of the modes in low spatial frequency harmonics. To this end, a metric on power distribution is introduced and used as a cost function for optimization using an iterative approach. Results, efficiency, robustness of the procedure and consequences of such optimization for both near-field and far-field with various structures and scenarios, are shown using both simulated and experimental data. All the data sets used for testing purposes, follow an *igloo* sampling scheme [12], defined by $\delta\varphi = \frac{\delta\theta}{\sin\theta}$ for a chosen angular step in θ, as it presents a quite uniform distribution of the samples over the sphere and are easy to go through for the positioning systems available at IETR.

The paper is organized as follows. First, we give theoretical insights about the VSH expansion, consequences of rotations/translations over the spectrum and techniques for spherical coefficients identification. Secondly, the proposed approach for optimizing the antenna position is described in Section III. Numerical results on near field are shown in IV and experimental ones in Section V. Finally, conclusions are drawn in Section VI.

II. Spherical Harmonic Spectrum of Antennas

A. Spherical Harmonic Expansion

1) General Formulation: The electric field $\mathbf{E}$ emitted by a radiating structure can be expanded outside the source region using Vector Spherical Harmonics (VSH) [1]:

$$\mathbf{E}(r,\theta,\varphi) = \frac{k}{\sqrt{\eta}} \sum_{smn} Q_{smn} \mathbf{F}_{smn}(r,\theta,\varphi) \tag{1}$$

with k the wavenumber, η the admittance of the propagation medium and (r,θ,φ) the spherical coordinates. The functions $\mathbf{F}_{smn}$ are the VSH and Q_{smn} the spherical coefficients. These complex quantities are a representation of the field $\mathbf{E}$ in a given coordinate system. The knowledge of these spherical coefficients enables computing the field everywhere outside the sphere centered at the origin and enclosing all the sources (spheres S and S', depending on the origin O or O', in Fig. 1). The index s represents the propagation mode of the VSH, transverse electric or magnetic. The indices n and m are respectively named the degree and the order. In practice, the series in (1) is truncated to $n \leq N$ according to the following empirical rule

$$N = \lfloor ka \rfloor + 10. \tag{2}$$

where a is radius of the minimum enclosing sphere S centered at the origin, as shown in Fig. 1 and $\lfloor x \rfloor$ the floor function. From this, we are able to compute the total radiated power as [1]:

$$P_{\text{rad}} = \frac{1}{2} \sum_{smn} |Q_{smn}|^2. \tag{3}$$

This formula can be generalized to compute the power contained in some part of the spectrum, as in [15] and further in this paper.

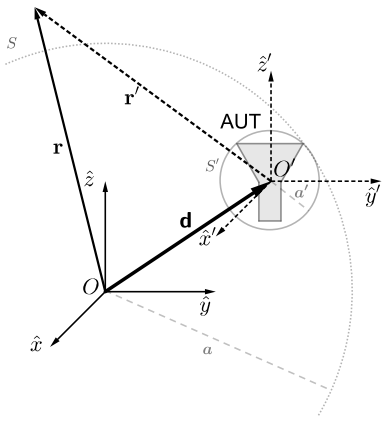

Fig. 1. Translation of the coordinate system by a vector $\mathbf{d}$. The corresponding minimal spheres enclosing the AUT are S, S' with radii a, a' respectively.

2) Spherical Coefficients Identification: An efficient and common way to derive the spherical coefficients Q_{smn} from field samples is by exact computation of integrals, which are projections of the discretized field into the VSH basis, using a Fourier Transform (FT) based method. This technique enables analytical results while being numerically stable [2]. However, it requires a significant amount of samples since the field must be known over an equiangular sampling because of the FT (constant steps in both angular coordinates $\delta\varphi$, $\delta\theta$). Besides, this constraint leads to a strong oversampling near the poles.

Another possibility is to formulate the truncated VSH expansion in (1) as a linear system of equations. Suppose the electric field radiated by the Antenna Under Test (AUT) is measured at M sampling positions over a sphere of radius R, $\mathbf{r}_i = (R,\theta_i,\varphi_i), i = 1,\ldots,M$. The electric field expansion (1) can thus be rewritten:

$$\mathbf{y} = \mathbf{A}\mathbf{x} \tag{4}$$

where $\mathbf{y}$ gathers the measurement data $\mathbf{E}(\mathbf{r}_i)$, of size $2M$ (two orthogonal polarization measurements per sampling point), $\mathbf{A}$ is the matrix containing the discretization of the VSH at the positions $\mathbf{r}_i$ and $\mathbf{x}$ contains the spherical coefficients Q_{smn}. The matrix has to be modified according to the transmission formula when dealing with near-field measurements to compensate for the probe radiation pattern [1].

The equation (4), when overdetermined (i.e. more field samples than unknown spherical coefficients), can be solved using the Truncated Singular Value Decomposition (TSVD) [16]. In an underdetermined scenario (less measurement data than unknowns), the sparsity of the SH coefficients $\mathbf{x}$ enables to find a solution nonetheless. A convex optimization problem, known as Basis Pursuit Denoising (BPDN) [17] has been applied successfully in fast spherical measurement techniques [9], [11]–[14] and is defined as

$$\min_{\mathbf{x}} \|\mathbf{x}\|_1 \text{ subject to } \|\mathbf{A}\mathbf{x} - \mathbf{y}\|_2 \leq \sigma, \tag{5}$$

where σ is the error tolerance parameter and $\|\mathbf{x}\|_1$ is the sum of the modulus of each component of $\mathbf{x}$. It can be solved efficiently using many readily available routines, such as the SPGL1 algorithm [18], [19]. The main advantage of this matrix formulation is the flexibility with respect to the field sampling scheme. However, caution must be taken to ensure the stability of the coefficient identification in undersampled cases. This exact point is discussed in Section II-C2.

B. Coordinate System Transformations

The spherical mode spectrum of the radiating structure depends on the position and orientation of the coordinate system of the expansion. The analytical formulas of rotation and translations are first recalled before investigating their impact on the VSH spectrum.

1) Analytical Formulas: A rotation or translation of a VSH leads to another function over the sphere, which can in turn be expanded into the VSH basis located around the new coordinate system. Let $\mathbf{r}$ the position in the measurement system and $\mathbf{r}_{\text{rot}}$ the position in the one rotated according to Euler's angle $(\varphi_0, \theta_0, \chi_0)$ in zyz convention, we have [1]:

$$\mathbf{F}_{smn}(\mathbf{r}) = \sum_{\mu=-n}^{n} D^n_{\mu m}(\chi_0, \theta_0, \varphi_0)\mathbf{F}_{s\mu n}(\mathbf{r}_{\text{rot}}) \tag{6}$$

where $D^n_{\mu m}$ are the Wigner D-functions.

Similarly, let us consider the translation with the case described in Fig. 1. The measurement coordinate system is centered at O with basis $\{\hat{x}, \hat{y}, \hat{z}\}$ and position vector $\mathbf{r}$. By translating it by a vector $\mathbf{d}$, we generate a new one, centered around O. Thus we define $\mathbf{d} = \overrightarrow{OO'}$ and this new coordinate system has basis $\{\hat{x}', \hat{y}', \hat{z}'\}$ with position vector $\mathbf{r}'$. The translation of the AUT can be achieved in two ways: moving the AUT with respect to the reference coordinate system (i.e. modifying the measurement data, vector $\mathbf{y}$ in (4)), or moving the reference system with respect to the AUT (i.e. transforming the VSH basis, matrix $\mathbf{A}$ in (4)). The second is achieved for translations over the z-axis if the displacement distance $\|\mathbf{d}\|$ is smaller than the observation distance $\|\mathbf{r}\|$, $\|\cdot\|$ being the Euclidean norm, by [1]:

$$\mathbf{F}_{s\mu n}(\mathbf{r}) = \sum_{\sigma=1}^{2} \sum_{\substack{\nu=|\mu| \\ \nu\neq 0}}^{\infty} C^{sn(1)}_{\sigma\mu\nu}(k\|\mathbf{d}\|)\mathbf{F}^{(c)}_{\sigma\mu\nu}(\mathbf{r}') \tag{7}$$

where $C^{sn(1)}_{\sigma\mu\nu}(k\|\mathbf{d}\|)$ are the translation coefficients depending on the distance and the measured frequency. An arbitrary displacement is achieved as a 3 step process:

1) A first rotation to align the translation vector with the z-axis.
2) A translation over the z-axis.
3) A second rotation to put the antenna back to its initial orientation.

Finally, possible uncertainties may be introduced if the truncation order of the series is not large enough when computing the translated VSH basis.

The transformation of the coordinate system tied to the AUT can be done more efficiently in far field since it boils down to a phase shift. Let us consider an arbitrary component (e.g. $\hat{\theta}$ or $\hat{\varphi}$ component) of the electric far field E with respect to the measurement basis around O. The same field component in the translated measurement system around O', as in Fig. 1, noted E_d is expressed [20], [21]:

$$E_d = Ee^{-jk\frac{\mathbf{r}'}{\|\mathbf{r}'\|}\cdot\mathbf{d}}, \tag{8}$$

where $\cdot$ is the scalar product. Note that amplitude and sampling positions changes have been neglected here. One can thus easily derive the electric far-field component E_d in any translated coordinate system. The modification of the VSH basis is more accurate as there is no approximation over amplitude or sampling positions changes. However, it requires more computational power. We are able to move the coordinate system at any position and orientation in the measurement sphere using the formulas above.

Both coordinate system transformations implies continuous changes over the spectrum: small translations or rotations induce small changes over the AUT spectrum. These effects can be harnessed in order to control, to some extent, the mode power distribution over the spectrum.

2) Influence on the VSH Spectrum: A translation of the coordinate system is known to generate modifications on the distribution of significant coefficients over both the degree n and the order m. More specifically, rotations have an impact only on the distribution over the orders m, as rotation of a VSH in (6) with given degree n is written using only VSH of the same degree n. These considerations are summed up in Fig. 2. As the order m satisfies $-n \leq m \leq n$ for VSH of degree n, the position of the origin is our only concern for power distribution over the degrees. The intuitive explanation is that any rotation around the origin does not change the radius of the minimum sphere enclosing the antenna under test and thus the truncation order N in (2) of the VSH series. Conversely, any translation does modify this radius and therefore N, as depicted in Fig. 1.

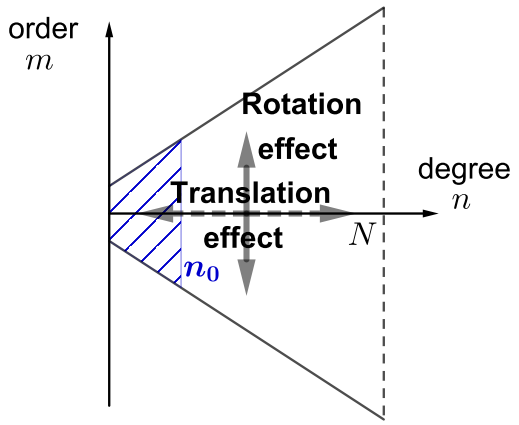

Fig. 2. Representation of a VSH spectrum and effects of coordinate system changes. Rotations will only have an effect over the orders m while translation impact both the orders and the degrees n. The dashed region represents the area of the spectrum where $n \leq n_0$.

We illustrate these effects using a simulation on HFSS of a horn antenna at 30 GHz. The far field is expanded on the VSH basis for several shifts of the antenna position over the z-axis by a step of a wavelength: at initial position (chosen close to its *a priori* phase center, between the imaginary apex point and the aperture [20]), and after translations of the coordinate system origin by $1, 2$ and 3 wavelengths λ on the z-axis. The spherical coefficients are displayed in Fig. 3. All those coefficient sets describe the same far field in magnitude, as only phase changes significantly, according to (8). Larger translations induce even more spread of the spectrum to higher degrees n. The same is done for the rotation of the AUT by random Euler's angle triplet, the result are displayed in Fig. 4. As claimed, there is no spread of the significant modes to larger degrees n but only over the orders m.

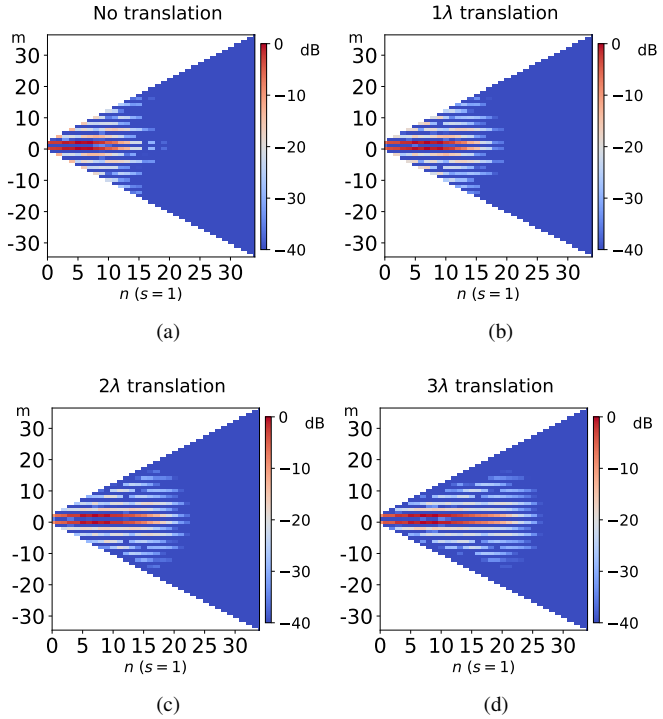

Fig. 3. Normalized spherical coefficients for $s = 1$ of the horn antenna at 30 GHz. Translations are performed along the z-axis.

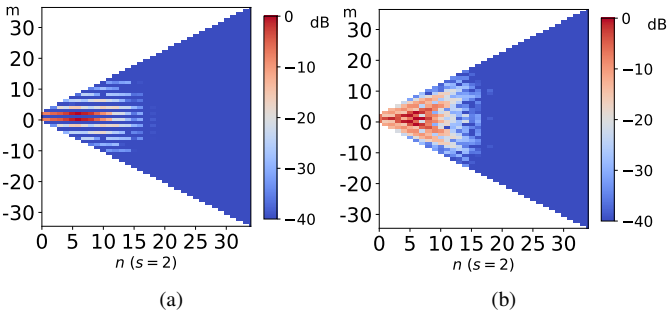

Fig. 4. Normalized spherical coefficients for $s = 2$ of the horn antenna at 30 GHz. Expansion in the initial coordinate system (a) and after rotation by random Euler's angle (b).

C. Spherical Modes Power Distribution

The transformation of the coordinate system modifies the power distribution over the VSH spectrum in both the order and the degree directions. We present a metric to quantify this distribution along the degree n.

1) The n-spectrum: The spectrum is truncated at a given degree N defined in (2). The power remaining for degrees $n \geq N$ in the spectrum must be negligible to ensure a proper characterization using the so-truncated series. This verification is called the N-test [1] and is based on the n-spectrum, the power radiated from VSH at a given degree n and is expressed as follows:

$$P(n) = \frac{1}{2} \sum_{sm} |Q_{smn}|^2 \tag{9}$$

As an illustrative example, let us consider a horn antenna simulated at 30 GHz, as before. We give in Fig. 5 the n-spectra corresponding to the spherical coefficients after various translations over the z-axis presented in Fig. 3. The 0λ case means that the origin is centered around the phase center. The spread of significant modes to higher degrees n leads to greater values of the n-spectrum, $P(n)$.

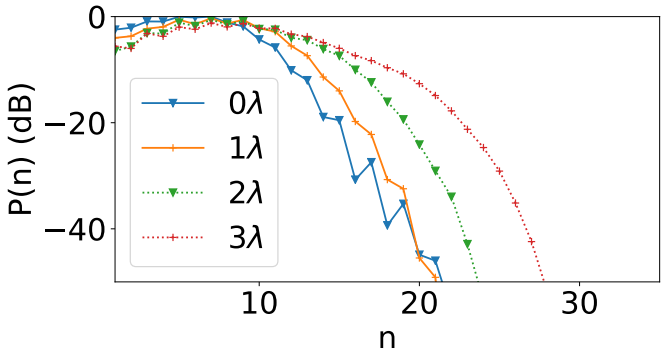

Fig. 5. Normalized n-spectra of the horn antenna at 30 GHz for different translations over the z-axis.

2) Advantages of Low Degree Modes: There are multiple reasons for promoting spectra with mode power distributions on low degrees. A faster decrease of the n-spectrum allows the reduction of the truncation order N, consequently requiring less field samples and reducing computational load. For example in Fig. 5 and a standard criterion of power below -40 dB, the horn properly positioned (no translation, 0λ) requires a minimum truncation order around $N = 20$, or 880 coefficients whereas the horn translated by a distance of 3λ needs at least $N = 27$, representing 1566 coefficients. Moreover, a low-degree spectrum induces a more compact representation of the antenna and is connected to the radiation center as explained in [15].

The modes having high-spatial frequencies, or equivalently high-degree VSH, require more field samples to achieve the same reconstruction accuracy relatively to low-frequency ones, especially for fast/undersampled measurements. As shown in [13], [14], the number of required field samples is linked to the sampling ratio, defined as the size of the dataset over the number of unknowns. If the actual power distribution can lead

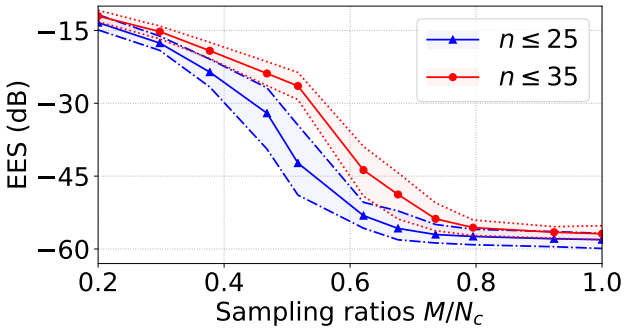

Fig. 6. Reconstruction accuracy in EES for 100 trials (median in plain lines and envelopes in dotted ones) for two spherical spectra families of same size N_c and number of non-zero coefficients (30 %) but different power distributions over the degrees n (constrained to $n \leq 25$ or $n \leq 35$) with respect to the sampling ratio M/N_c, M the size of the field sample used for recovery.

to a reduction of the truncation order (e.g. by a N-test), the number of unknowns decreases and fewer samples are thus required to achieve the same sampling ratio.

We illustrate this statement by randomly generating two families of 100 spherical coefficients spectra having the same total number of coefficients N_c, truncation order of $N = 45$, and non-zero coefficients (30 %). Non-zero coefficients are drawn over the degrees $n \leq 25$ for the first family and $n \leq 35$ for the second one so the only difference between the two families is the power distribution constraint over the degree. Using BPDN in (5), we recover each spectrum using far-field samples of different sizes M, or sampling ratio M/N_c. The accuracy of the recovered spectrum is assessed by comparing the reconstructed far-field from the M field samples to the one directly generated by the randomly drawn spectrum. This comparison is achieved using the Equivalent Error Signal (EES), defined as a mean relative error in dB between a reference $\mathbf{y}$ and its estimation $\widetilde{\mathbf{y}}$, both of size M:

$$\mathrm{EES}(\mathbf{y}, \widetilde{\mathbf{y}}) = 20 \log_{10} \left(\frac{\|\mathbf{y} - \widetilde{\mathbf{y}}\|_1}{M \|\mathbf{y}\|_\infty} \right). \tag{10}$$

where $\|\mathbf{y}\|_\infty$ is the maximum modulus among each of the components of $\mathbf{y}$. The results are displayed in Fig. 6.

As an example, a field sampling ratio $M/N_c = 60\%$ is enough for all 100 trials of the low-frequency family ($n \leq 25$) to achieve a reconstruction accuracy of -45 dB in EES. Conversely, the high-frequency one ($n \leq 35$) never achieved this accuracy for this sampling ratio and required around 70 % to perform equally well. This trend is expressed over all the sampling ratios as the median values of reconstruction accuracy in EES is always better for the lower frequency spectra using the same sampling ratio, while there was as many non-zero spherical coefficients to retrieve in both cases.

III. Determination of the Antenna Position

We propose an optimization algorithm to exploit the coordinate system position in order to improve the characterization of antennas.

A. Optimization Problem

A simple criterion is presented to characterize the power distribution over the degrees. This criterion will then be used as an objective function in order to foster a low-degree spectrum.

1) The cumulative n-spectrum: The cumulative n-spectrum is defined for all degrees n lower than the truncation order. Its value at a given degree n_0 contains the power of all modes of degrees $n \leq n_0$, the region illustrated by the dashed area in Fig. 2. We consider the normalized version, allowing a constant scale, which is omitted in the name for convenience and is given by

$$H(n_0) = \frac{1}{P_{\text{rad}}} \sum_{n=1}^{n_0} P(n). \tag{11}$$

As a cumulative normalized function, it is increasing towards 1. A faster decrease of the power in the n-spectrum leads to a cumulative spectrum reaching 1 more quickly, as illustrated in Fig. 7, corresponding to the n-spectra of the horn at 30 GHz for several positions shown in Fig. 5 and the spectra in Fig. 3.

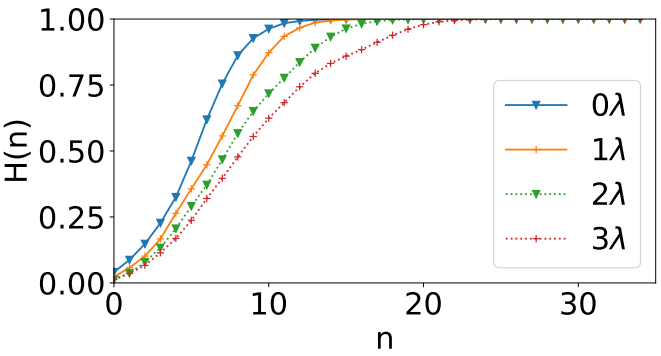

Fig. 7. Cumulative n-spectra H of the horn antenna at 30 GHz for different translations over the z-axis. A better concentration on low degrees n modes makes the curve approaching 1 for lower n-values.

A cumulative spectrum can be associated to a mean value, which is defined by

$$\langle \mathbf{H} \rangle = \frac{1}{N-1} \sum_{n=1}^{N-1} H(n). \tag{12}$$

It is clear that a cumulative spectrum converging quickly to 1 has a larger mean value. Mean values for the cumulative spectrum curves of the horn in Fig. 7 are shown in Table I. We do not consider the last value $H(N)$ as it is always equal to 1.

In order to better emphasize the contrast between the cumulative spectra and to help the choice of the best antenna position, we replace H by a modified version defined as:

$$H_{\text{mod}}(n) = 10 \log_{10} \left[\frac{n}{N} (1 - H(n)) \right]. \tag{13}$$

Working on $1 - H(n)$ maps the increase towards 1 of the cumulative spectrum function to a decrease to 0, where values can be better discriminated by the logarithmic scale. The multiplication by n/N accounts for the number of VSH of

same degree n while keeping the values in the interval $[0, 1]$. The values of the cumulative spectrum and its modified version are reported in Table I for the horn simulated at 30 GHz, showing the improvements in the discrimination of high-frequency content of this adapted metric.

TABLE I
MEANS OF THE CUMULATIVES n-SPECTRA OF THE HORN AT 30 GHZ FOR SEVERAL TRANSLATIONS OVER THE z-AXIS

Translation Distance	0λ	1λ	2λ	3λ
$\langle \mathbf{H} \rangle$	0.84	0.80	0.77	0.73
$\langle \mathbf{H}_{\text{mod}} \rangle$	-69.1	-67.7	-52.4	-24.1

2) Formulation of the Optimization Problem: The concentration of the power distribution to the low-degree part is achieved by a minimization of the cumulative n-spectrum on the modified scale. Given a translation $\mathbf{d}$ of the AUT relatively to the origin of the measurement coordinate system, as in Fig. 1, we identify the spectrum $\mathbf{Q_d}$ with the method of our choice (analytical projection or numerical inversion), enabling the evaluation of the cumulative n-spectrum and therefore its mean value, denoted $\langle \mathbf{H}_{\text{mod}} \rangle(\mathbf{Q_d})$. This can be summed up in the following optimization problem:

$$\min_{\mathbf{d}} \ \langle \mathbf{H}_{\text{mod}} \rangle(\mathbf{Q_d}). \tag{14}$$

The solution of this optimization problem is an estimation of the *best* translation to apply to the antenna under test leading to the highest concentration of the radiated power on the low degree part according to our metric. This solution is denoted $\mathbf{d}^*$.

Note that in the case of a numerical inversion to find the spectrum $\mathbf{Q_d}$, two situations can be distinguished to get the matrix formulation (4) after a translation $\mathbf{d}$:

- $\mathbf{A_d x} = \mathbf{y}$ with near or far-field data, with $\mathbf{A_d}$ the translated version of the VSH contained in $\mathbf{A}$.
- $\mathbf{Ax} = \mathbf{y_d}$ where $\mathbf{y_d}$ contains electric far-field data and computed according to (8).

No further measurements are required after optimization: once $\mathbf{Q_d}$ is found, we can reconstruct the field in the measurement coordinate system either by computing $\mathbf{B_d Q_d}$ for the first approach, like in [8], or $\mathbf{BQ_d} = \mathbf{z}$ and taking $\mathbf{z}_{-d}$ according to (8) for the second one, $\mathbf{B}, \mathbf{B_d}$ being the VSH matrix over the reconstruction sampling and its translated version, respectively.

B. Practical Resolution

We present an iterative algorithm to solve the previously described optimization problem and find the antenna position that concentrates the significant spherical modes on the low degrees.

1) Gradient Descent Algorithm: The optimization of the position, or equivalently the translation $\mathbf{d}$ from the measurement coordinate system, using (13) or (14) is not a convex problem and cannot be solved easily. We propose to find an approximated solution of these optimization problems, $\mathbf{d}^*$, using a gradient descent technique. This iterative algorithm follows the negative (approximated) gradient of the objective function, $\langle \mathbf{H}_{\text{mod}} \rangle(\mathbf{Q_d})$. The detailed procedure is given in Algorithm 1. The proposed approach is general and can be applied with no modification to all spherical coefficient identification methods (analytical and numerical ones) and is valid for both near-field and far-field measurements.

Algorithm 1 Concentration of the spherical spectrum power distribution to low degrees

Require: δ the perturbation step, μ the gradient multiplier, $\mathbf{d}_0$ the initialization point.

Initialization
$\mathbf{d} \leftarrow \mathbf{d}_0$
while Stopping criterion not met **do**
  Apply the translation $\mathbf{d}$
  Compute the spherical coefficients at $\mathbf{d}$
  Evaluate $\langle \mathbf{H}_{\text{mod}} \rangle(\mathbf{Q_d})$
  $\#$ *Computation of the numerical gradient* $\mathbf{D}$
  for $\hat{u} = \hat{x}, \hat{y}, \hat{z}$ **do**
    $\mathbf{d}_{\hat{u}} \leftarrow \mathbf{d} + \delta\hat{u}$
    Compute spherical coefficients at $\mathbf{d}_{\hat{u}}$
    Evaluating $\langle \mathbf{H}_{\text{mod}} \rangle(\mathbf{Q}_{\mathbf{d}_{\hat{u}}})$
    $D_{\hat{u}} \leftarrow [\langle \mathbf{H}_{\text{mod}} \rangle(\mathbf{Q}_{\mathbf{d}_{\hat{u}}}) - \langle \mathbf{H}_{\text{mod}} \rangle(\mathbf{Q_d})] / \delta$
  $\mathbf{D} \leftarrow [D_{\hat{x}}, D_{\hat{y}}, D_{\hat{z}}]^T$
  $\#$ *Position Update*
  $\mathbf{d} \leftarrow \mathbf{d} - \mu\mathbf{D}$
return $\mathbf{d}$

2) Implementation Details: The perturbation step δ is the (small) change applied to the translation for approximating the gradient of the metric. This value has to be chosen relatively to the expected accuracy of the measurement system configuration to generate perturbations that are meaningful with respect to the available data. A too small δ will result in a noisy and unstable estimation. Conversely, a too large δ leads to unfaithful and too coarse gradient evaluation. A value of $\delta = 0.5$ mm has been successfully used in all presented cases. The gradient multiplier μ is a constant chosen in order to avoid large updates of $\mathbf{d}$ within one iteration by a relevant re-scaling of the gradient. It should be fixed so the position update is not too large in terms of wavelength or with respect to the tested structure to ensure proper convergence of the algorithm. A value $\mu \approx 10^{-5}$ for normalized data ($\|\mathbf{y}\| = 1$) leads to updates around several millimeters for most cases.

The initialization point $\mathbf{d}_0$ in Algorithm 1 can be set using various methods. A starting value $\mathbf{d}_0 = \mathbf{0}$ means that it starts from the origin of the measurement coordinate system. It can also be chosen randomly or one can provide an initial guess based on some prior knowledge, e.g. the known position of the AUT geometrical center with respect to the measurement coordinate system.

Multiple stopping criteria can also be chosen. One can use the difference of the cost function between two or more iterations, the decrease of the cost function below a predefined threshold or define a maximum distance for the translation $\mathbf{d}$, (for example with respect to the wavelength or the dimensions of the antenna), or a predefined number of iterations.

With proper parameter tuning, a notable reduction of the objective function has been achieved within only a few iterations for all investigated cases. The translation corresponding to the lowest value of the cost function should be kept.

IV. Numerical Validations at Near-Field of Radiating Structures

The proposed approach is applied on various radiating structures, whose near field is computed by CST MWS.

A. 11-Patch Array at 9.5 GHz

We consider a linear array composed of 11 patches operating in X band at 9.5 GHz, as illustrated in Fig. 8. Each square patch has side length 10 mm and the overall size of the array is 165 mm ($\approx 5.25\lambda$), the electric near field is exported from CST at 200 mm from the geometric center. As illustrated, not all patches are fed with the same amplitude. The left patch is not receiving any power and the feeding is increasing as we go to the right patch in order to generate an asymmetric current distribution. Taking the geometric center of the array as the origin yields the spectra (a) displayed in Fig.9 while the optimized position yields the ones in (b). If the geometric center of the antenna is considered as the center of the measurement coordinate system, the proposed algorithm finds the optimized coordinate system origin to be at $\mathbf{d}^* = (0.6, 18.7, 2.1)$ mm, meaning that it is shifted towards the area containing most part of the electric current density while preserving the symmetry around the x-axis, the orthogonal direction to the array, with a very small shift of less than $\lambda/50$. No additional knowledge or data has been used in the process, the optimization being started from the geometric center of the array with the corresponding field values. The AUT position optimization process took about 52 s on an Intel i7 8700 with 16 GB RAM.

The optimized coordinate system position enables not only to significantly reduce the amount of significant spherical harmonic coefficients but also to concentrate them to low degree modes as displayed in Fig. 9. The truncation order is $N = 27$, or 1566 coefficients and a field sample along an *igloo* sampling of size 900 is taken to generate a very coarse measurement set and is used for both position optimization and reconstruction. Reconstruction accuracy from the same initial data set with respect to the reference (the electric spherical near-field exported from CST over a dense set of points) are evaluated by EES values (10) of -44.8 dB for the geometric center and -58.9 dB for the optimized position.

B. Antenna on satellite structure at 11 GHz

As a study case, a single rectangular patch is now placed on a platform of a satellite ANGELS [22] (the real payload being a different antenna), the whole structure is displayed in Fig. 10 and we exploit the simulated spherical near field simulated at 5 m from the measurement coordinate system, supposed at the center of the satellite's body for practical reasons: cinematic or weight for instance. The minimum sphere is set to enclose the satellite body and some part of the solar panels, leading

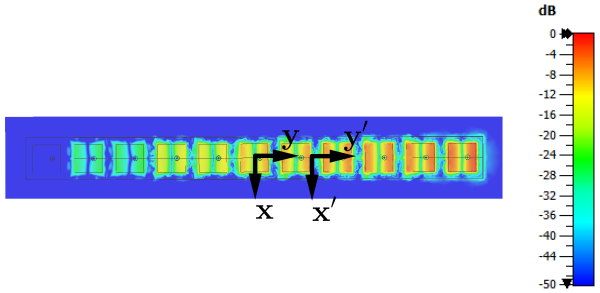

Fig. 8. Surface currents normalized amplitude of the 11-patch array (value averaged over one phase cycle): measurement coordinate system $(\mathbf{x}, \mathbf{y})$ (geometric center) and optimized one $(\mathbf{x}', \mathbf{y}')$.

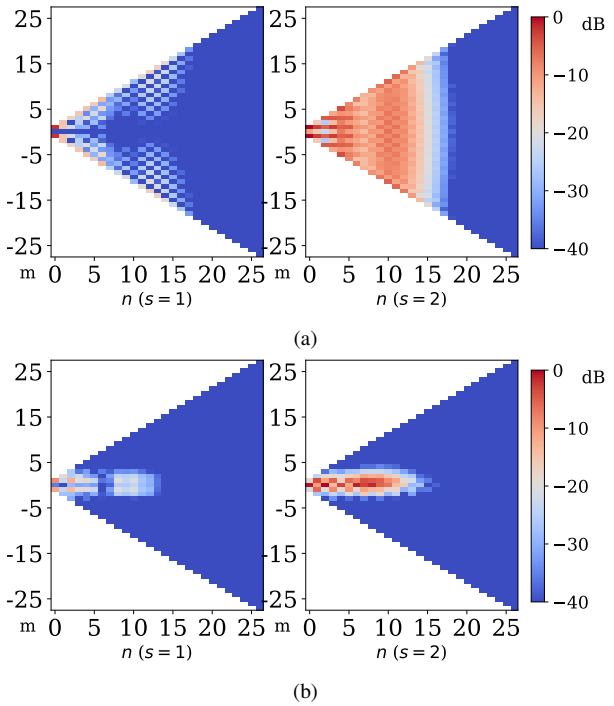

Fig. 9. Normalized spherical coefficients of the patch array: (a) with origin at the geometric center, (b) with optimized position.

to 6726 spherical coefficients. The data set comes from a field sample of size 1700 along an *igloo* sampling so there are enough data with respect to the patch alone while still having a largely underdetermined linear system to cope with.

The geometric center of the antenna is located at $\mathbf{d}^c = (0, 120, 113)$ mm, which corresponds to a distance of approximately 6λ. The optimization process starts from the center of the satellite and converges to an optimized position of $\mathbf{d}^* = (0.3, 125.6, 102.9)$ mm that turns out to be fairly close to the antenna geometric center. The spectra are represented in Fig. 11 and the modified cumulative n-spectra $\mathbf{H}_{\mathrm{mod}}$ are shown in Fig. 12. The returned optimized position is close but not equal to the geometric center, resulting in a different power distribution. Indeed, we observe more power at very low degrees when centered at the antenna but the optimized position allows a faster decrease of the contained power for degrees $n \geq 10$, allowing for a slightly more accurate far-field reconstruction for the considered data. The obtained EES of

the reconstructed field from the same initial data over a dense reference sampling are respectively -43.1 dB and -43.6 dB for the centered on the antenna and the optimized position from the center of the satellite.

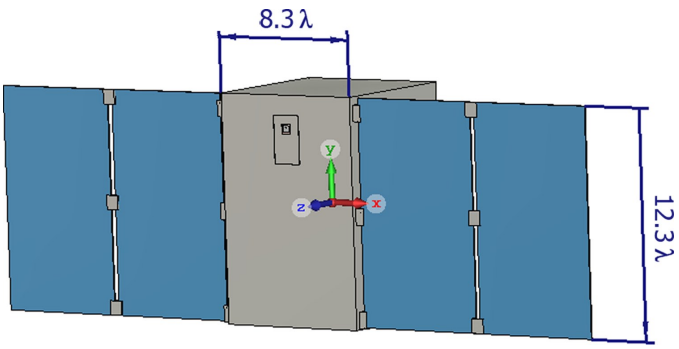

Fig. 10. Simulated model of the antenna (a patch) on a platform satellite (a simplified version of ANGELS) with the patch antenna at 11 GHz and the measurement coordinate system.

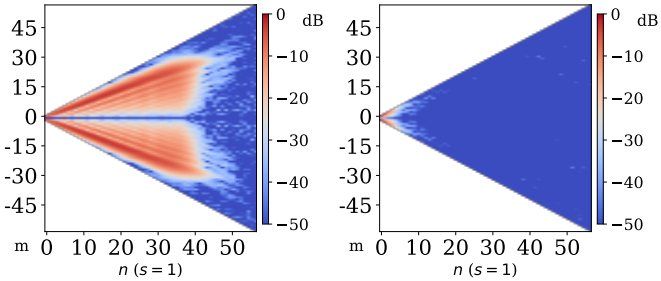

Fig. 11. Normalized spherical coefficients for $s = 2$ of the mounted patch at 11 GHz: (a) measurement coordinate system, (b) optimized position.

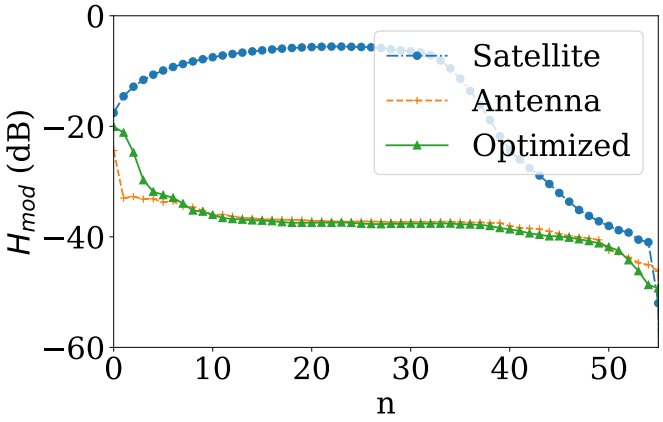

Fig. 12. Modified scale of the cumulative n-spectra for the initial measurement origin, centered on the antenna and with optimized position.

C. Discussion

The geometry of the radiating structure does not always help the choice of origin for the VSH basis. In the patch array case, various excitation patterns induce very different ideal coordinate system positions. We are able to automatically determine the position leading to a high concentration of the spectrum over the low-degree modes without any knowledge of the structure apart from its maximum dimension and measured frequency in order to set the truncation order of the VSH series. It is of great interest for reconfigurable antennas, where several operating modes can be tested accurately without having to move the antenna physically. In the case of the antenna embedded on a satellite, the procedure finds automatically the *best* position (according to our metric), at a distance of around 6 λ from the measurement position. This optimized position yields a slight improvement of the pattern reconstruction and confirm the stability of the proposed procedure. Indeed, despite having a small number of measurement samples with respect to the spherical coefficients to be determined, the necessary large translation of the antenna under test is properly predicted.

These representative cases demonstrate the robustness of the proposed approach as well as its practical relevance. The proposed procedure enables to compensate automatically uncertainties on the antenna position with respect to the measurement system. It also allows to accurately position embedded antennas when the interaction between the radiator and its structure cannot be neglected.

V. Experimental Validations at Far-Field of Radiating Structures

Let us now consider far-field measurements of various radiating structures that have been carried out in far-field anechoic chambers of the M^{2}ARS facilities at IETR. They are equipped with a roll-over-azimuth positioning system and a mechanical probe polarization change. The field is acquired step by step following an *igloo* strategy [12].

A. Position optimization

Two antenna far-field measurements, carried out over an hemisphere using a low-density sampling, are presented here. The reference is provided by a measurement of a densely sampled cutting plane. Since the sampling positions only cover a hemisphere in far field, we can restrict ourselves to $\mathbf{F}_{smn}$ such that $n + m$ is even. By assuming the symmetry of the radiation pattern with respect to the equator, all the spherical coefficients Q_{smn} such that $m + n$ is odd are necessarily zero, further reducing the number of samples required to characterize the radiation pattern over the measurement region.

1) Leaky Wave Antenna (LWA) in K Band: The AUT is a LWA measured at 18 GHz (based on [23]) We compare the reconstruction of the field over the cutting plane $\varphi = 90°$ for the measurement coordinate system origin and the optimized position using the proposed approach. The antenna has a radius of $a = 15$ cm, leading to a truncation order of $N = 65$ hence 4420 even spherical coefficients to retrieve. The measurement data is along an *igloo* sampling and has size 3458, leading to a sampling ratio of 78 %, slightly above the 75 % required by our previous study for fast measurements in [24]. The usual method in [1] would have required a data set of size around 1.7×10^4.

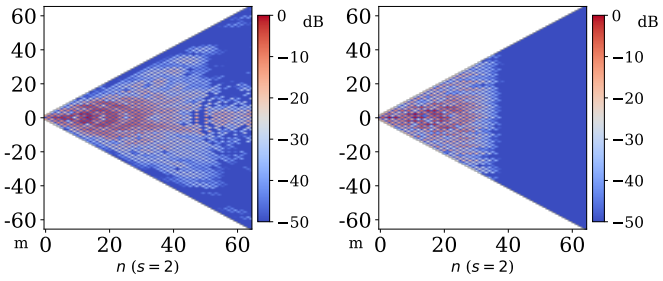

Fig. 13. Normalized spherical coefficients for $s = 2$ of the LWA at 18 GHz for the measurement coordinate system origin position (a) and with optimized position (b).

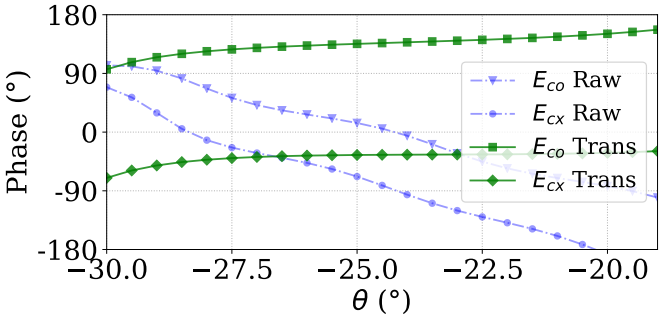

Fig. 15. Phases of the reconstructed fields co- and cross-polarization components around main lobe over the cutting plane $\varphi = 90°$ degrees of the LWA at 18 GHz .

The spherical coefficients for one propagating mode s are displayed in Fig. 13, leading to the objective function $\langle \mathbf{H}_{\text{mod}} \rangle$ values of -11.2 dB and -39.5 dB with a proportion of significant coefficients being 54 % and 27 % respectively. The cutting plane for comparison to reference is shown in Fig. 14. We observe a much better agreement of the field reconstruction when optimizing the position of the antenna. The reconstructed field phases around the main beam angular zone are plotted in Fig. 15, we note that they have been smoothed out significantly after the proposed procedure. Using the data phase-shift equation (8) for optimizing the AUT position, the optimization process took 47 s on an Intel i7 8700 with 16 GB Ram.

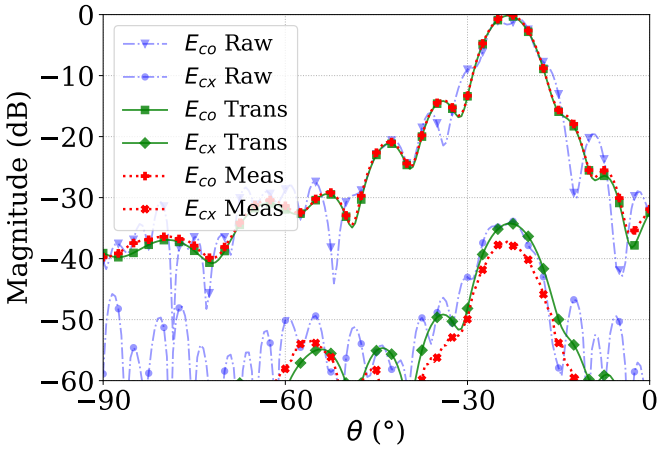

Fig. 14. Normalized magnitude of the field co- and cross-polarization components over the cutting plane $\varphi = 90°$ of the LWA at 18 GHz .

2) Circularly polarized horn antenna at 320 GHz*:* This antenna [25] has been measured along a coarse sampling over the hemisphere at 320 GHz. We use the same methodology as the previous one with a cutting plane at $\varphi = 0°$. The minimal sphere leads to a truncation order of $N = 50$, hence 2650 even coefficients. The measurement data set have been measured along an *igloo* sampling and has size 2122, corresponding to a sampling ratio $\approx 80\%$. The usual method in [1] would have required a data set of size around 10^4.

The spherical coefficients for one propagating mode s for measurement and optimized positions are displayed in Fig. 16, leading to objective function $\langle \mathbf{H}_{\text{mod}} \rangle$ values of -22.2 dB and -26.6 dB with proportion of significant coefficients of 15 % and 6 % respectively. The cutting plane in magnitude for comparison to the reference is shown in Fig. 17. The reconstructed field phases around the main beam angular zone are plotted in Fig. 18, the optimized antenna position leads, here as well, to smoother phase variations.

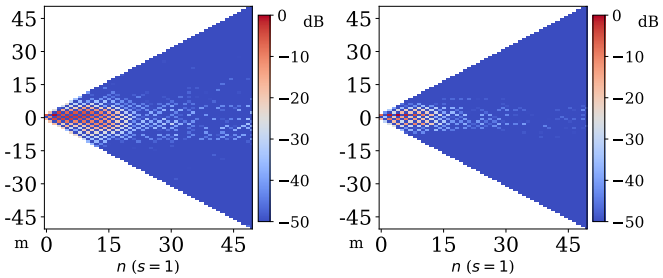

Fig. 16. Normalized spherical coefficients for $s = 1$ of the horn at 320 GHz for the measurement coordinate system origin position (a) and with optimized position (b).

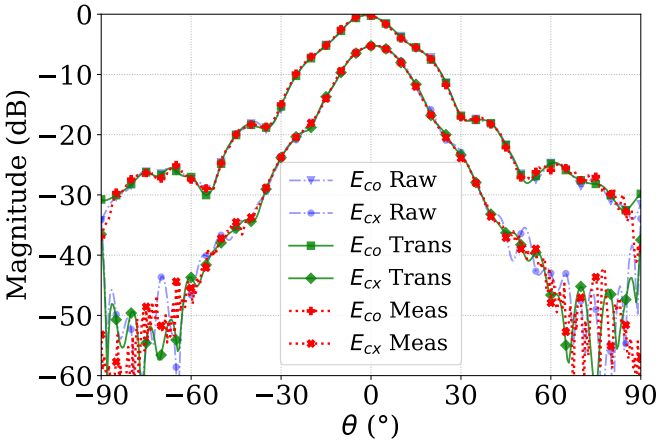

Fig. 17. Normalized magnitude of the field co- and cross-polarization components over the cutting plane $\varphi = 0$ degrees of the horn at 320 GHz.

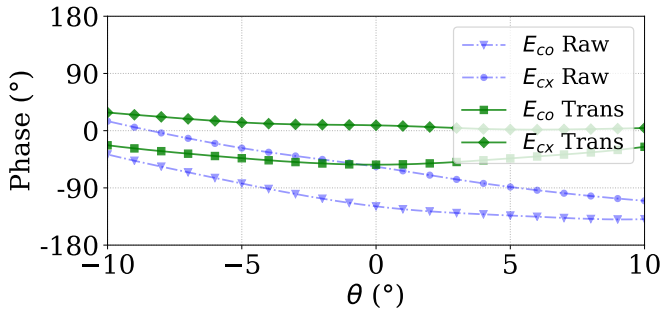

Fig. 18. Phases of the reconstructed fields co- and cross-polarization components around main lobe over the cutting plane $\varphi = 0$ degrees the horn at 320 GHz.

B. Discussion

The concentration of the spectrum in low-degree modes has been achieved in both cases as shown by the spectra. This leads to significant improvements in the field reconstruction from a given initial undersampled far-field data set and thereby validates experimentally our approach. We have also noticed that the antenna position optimization leads to smooth out the phase variations over the main beam. This particular point is described in [15], [26] and referred to as the antenna radiation center, the virtual point from which the main beam of the antenna is emitted.

VI. Conclusion

A procedure that processes radiation pattern measurements so as to find the *best* position of the antenna under test has been proposed. The underlying idea is to exploit at best the valuable information encompassed in the spherical harmonic spectrum of the antenna. By properly translating the antenna with respect to the measurement coordinate system, it is possible to concentrate the power of its spectrum to low frequency content. For that purpose, a metric based on the n-spectrum has been developed and integrated to an efficient optimization strategy. The proposed approach induces not only lower truncation orders for the spherical harmonic series but also better 3D radiation pattern reconstructions. It also diminishes the impact of an eventually bad AUT positioning in terms of power distribution among the spectrum. The procedure has first been validated numerically on the simulated near field of various radiating structures including an antenna embedded on a simplified satellite model. The far-field measurements of a reflectarray antenna in Ku band and a horn operating at THz frequencies have also been provided to further demonstrate the potential of the proposed strategy, always leading to an improved reconstruction of the radiation patterns from the same measurement data set.

References

[1] J. Hald, J. Hansen, F. Jensen, and F. Larsen, *Spherical Near Field Antenna Measurements*. Peter Peregrinus, 1988.

[2] O. Breinbjerg, "Spherical near-field antenna measurements — the most accurate antenna measurement technique," in *2016 IEEE International Symposium on Antennas and Propagation (APSURSI)*, June 2016, pp. 1019–1020.

[3] "Ieee recommended practice for near-field antenna measurements," *IEEE Std 1720-2012*, pp. 1–102, 2012.

[4] F. Jensen and A. Frandsen, "On the number of modes in spherical wave expansions," in *AMTA 2004*, October.

[5] R. Cornelius and D. Heberling, "Spherical wave expansion with arbitrary origin for near-field antenna measurements," *IEEE Transactions on Antennas and Propagation*, vol. 65, no. 8, pp. 4385–4388, Aug 2017.

[6] L. J. Foged, F. Saccardi, F. Mioc, and P. O. Iversen, "Spherical near field offset measurements using downsampled acquisition and advanced nf/ff transformation algorithm," in *2016 10th European Conference on Antennas and Propagation (EuCAP)*, pp. 1–3.

[7] F. D'Agostino, F. Ferrara, C. Gennarelli, R. Guerriero, and M. Migliozzi, "Reconstruction of the far field radiated by an offset mounted volumetric aut from non-redundant spherical spiral near-field measurements," *IET Microwaves, Antennas Propagation*, vol. 14, no. 14, pp. 1711–1718, 2020.

[8] F. Rodriguez-Varela, B. Galocha-Iraguen, and M. Sierra-Castañer, "Fast spherical near-field to far-field transformation for offset-mounted antenna measurements," *IEEE Antennas and Wireless Propagation Letters*, pp. 1–1, 2020.

[9] D. Loschenbrand and C. Mecklenbrauker, "Fast antenna characterization via a sparse spherical multipole expansion." Aachen: 4th International Workshop on Compressed Sensing Theory and its Applications to Radar, Sonar and Remote, 2016.

[10] D. L. Donoho and J. Tanner, "Precise undersampling theorems," *Proceedings of the IEEE*, vol. 98, no. 6, pp. 913–924, June 2010.

[11] C. Culotta-Lopez, D. Heberling, A. Bangun, A. Behboodi, and R. Mathar, "A compressed sampling for spherical near-field measurements," in *AMTA 2018*, Williamsburg Virginia, USA, Nov.

[12] B. Fuchs, L. Le Coq, S. Rondineau, and M. Migliore, "Fast antenna far field characterization via sparse spherical harmonic expansion," *IEEE Trans. Antennas Propag.*, vol. 65, no. 10, pp. 5503–5510, Oct. 2017.

[13] B. Hofmann, O. Neitz, and T. F. Eibert, "On the minimum number of samples for sparse recovery in spherical antenna near-field measurements," *IEEE Trans. on Antennas and Propag.*, July 2019.

[14] N. Mézières, B. Fuchs, L. Le Coq, J.-M. Lerat, R. Contreres, and G. L. Fur, "On the application of sparse spherical harmonic expansion for fast antenna far field measurements," *IEEE Antennas and Wireless Propagation Letters*, 2020.

[15] C. Culotta-Lopez, K. Wu, and D. Heberling, "Radiation center estimation from near-field data using a direct and an iterative approach," in *AMTA 2017*, Oct, pp. 1–6.

[16] G. H. Golub and C. F. Van Loan, *Matrix Computations*, 3rd ed. The Johns Hopkins University Press, 1996.

[17] M. Elad, *Sparse and Redundant Representations - From Theory to Applications in Signal and Image Processing*. Springer, 2010.

[18] E. van den Berg and M. P. Friedlander, "Probing the pareto frontier for basis pursuit solutions," *SIAM Journal on Scientific Computing*, vol. 31, no. 2, pp. 890–912, 2008. [Online]. Available: https://epubs.siam.org/doi/10.1137/080714488

[19] ——, "SPGL1: A solver for large-scale sparse reconstruction," June 2007.

[20] C. A. Balanis, *Antenna Theory: Analysis and Design*. Wiley-Interscience, 2005.

[21] S. McBride, D. Tammen, and W. Hess, "Best-fit 3d phase-center determination and adjusment," in *AMTA 2013*. NSI-MI Technologies.

[22] R. Fragnier, L. Feat, R. Contreres, B. Palacin, K. Elis, A. Bellion, and G. L. Fur, "Collocated compact uhf and l-band antenna for nanosatellite argos program," in *2019 13th European Conference on Antennas and Propagation (EuCAP)*, 2019.

[23] A. Dorlé, R. Gillard, E. Menargues, M. v. der Vorst, E. de Rijk, P. Martín-Iglesias, and M. García-Vigueras, "Sidelobe level reduction in ridged leaky waveguide through stereolithography," in *2019 13th European Conference on Antennas and Propagation (EuCAP)*, 2019, pp. 1–5.

[24] N. Mézières, B. Fuchs, L. Le Coq, J.-M. Lerat, R. Contreres, and G. L. Fur, "Fast antenna characterization improvement by pattern rotations," *IEEE Trans. on Antennas and Prop. (submitted)*, 2020.

[25] B. Aqlan, M. Himdi, L. Le Coq, and H. Vettikalladi, "Sub-thz circularly polarized horn antenna using wire electrical discharge machining for 6g wireless communications," *IEEE Access*, vol. 8, pp. 117 245–117 252, 2020.

[26] J. Fridén and G. Kristensson, "Calculation of antenna radiation center using angular momentum," *IEEE Transactions on Antennas and Propagation*, vol. 61, no. 12, pp. 5923–5930, 2013.